Chapter 4

Control Pulse Cleaning

4.1 Introduction

Quantum control experiments performed with evolutionary algorithms achieved impressive results in recent years [4, 5, 6], but on the other hand still suffer the consequences of the randomness of the employed search strategies. For example, the second major goal of optimal control theory and experiments is "learning" from the optimal solutions instead of purely influencing and "optimizing" molecular dynamics. A valid interpretation strongly relies upon reproducibility, accuracy, and a proper interpretation of the optimal light field's temporal and spectral features. Unfortunately, many things can go wrong, as experimental conditions vary and search algorithms may end up in local optima and there may be numerous other misjudgements in the general architecture and assumptions of experiment or algorithm. Additionally, problems with (possible multiple) local optima, combined with a considerable amount of noise might cause solutions not to comply with the desired reproducibility, robustness, power expenditure, or stability requirements. By repeating feedback-loop experiments many times, key features that are commonly found in the acquired data can be distinguished from random features, but still, the impact of features on the overall optimization factor is hard to determine. This is also partially due to the fact that it is still difficult to experimentally conduct "perfect" pulse shaping, and variations of certain parameters (particularly in the time domain) are predestined to produce more unwanted artifacts as pulse forms become more complex. As a consequence, unnecessary features might aggravate interpretation and theoretical analysis to a degree of uselessness because one can be easily fooled by apparent, major features of a waveform [73], if the search algorithm does not see any particular advantage in removing them, which is generally applicable: This type of search strategy will yield random values for genes/parameters, which do not obstruct the overall optimization goal.

Particularly, for free optimization performed with liquid crystal modulators, where a parameter-per-pixel-encoding is chosen, there is little else to adjust, except for the inner workings of the algorithm. It is, however, difficult to predict what the consequences of tuning (e.g. mutational and crossover rate, method of selection, etc.) will be as this can be regarded as a quite blindfold adaptation of metaheuristics. Even if the consequences were to provide for example more robustness, there is no telling if only a particular problem is addressed and enhanced and another

impaired[1].

Another possibility is tailoring the environment by redefining search space towards user-specific goals wherein individuals of the evolutionary algorithm compete for survival, which has the disadvantage that a reasonable ansatz to reshape the search space is required [75, 76].

An alternative approach, which is presented in this chapter, interferes in the selection process and gives individuals a "push" which satisfy particular user-defined goals. These goals can be constructed to eliminate unnecessary features, just like biological evolution removes unnecessary features on the long run: for example body parts due to their energy consumption and increased risk of disease.

The deterministic individual selection process used throughout this work takes a fixed number of individuals whose fitness values are highest to the next generation, and discards the rest. As this process is solely fitness dependent, this is the place to intervene for the so-called "control pulse cleaning". This method of manipulating the fitness is a cost-functional which adds an additional cost. Such a cost can be made dependent on various physically or practically motivated goals such as robustness, simplicity, or even performance under pressure. Implementing such concerns via the fitness was first suggested for the field of femtochemistry by Rabitz et al. in a theoretical study [73]. In this chapter, the first experimental demonstration of this concept in coherent control will be presented by eliminating less important transition frequencies for a three-photonic ionization of the NaK molecule.

4.1.1 Overview of the NaK molecule

In recent years, the sodium-potassium molecule, as a model-system alkali dimer, has been studied extensively by means of coherent control [36, 55], first by pump-probe spectroscopy and then by closed-loop experiments under numerous aspects such as frequency dependent optimization [77].

The first investigations [22, 23] of the molecular potentials lead to an oscillation period of a wavepacket in the first excited $A^1\Sigma^+$ state of T_{osc}=440 fs (see Fig. 4.1). Today, the molecular potentials are well known [78] and were extended to the cationic ground state [79]. The main results were an achieved controllability of the wavepacket dynamics of ionization [24, 25, 26, 27], fragmentation from Na_2K [36], and controlled ionization/fragmentation of the two most abundant isotopes $^{23}Na^{39}K$ and $^{23}Na^{41}K$ [80]. Phase-only optimization brought an ionization efficiency increase of 1.6 compared to an unshaped pulse [81]. This optimized pulse form featured sub pulse distances of about 220 fs and 660 fs, which was assigned to a wavepacket propagation on the $A^1\Sigma^+$ state, leading to a simple model for ionization, with a one-photon electronic transition from the ground to the excited state, followed a two-photon ionization from the outer turning point. A joint experimental-theoretical investigation provided deeper insight into the wavepacket dynamics, where wavepacket propagation on the intermediate $B(3)^1\Pi$ state was found to contribute as well [79].

[1] which is expressed by the famous "No-Free-Lunch theorem of optimization" [74], one of the most cited single works in the field

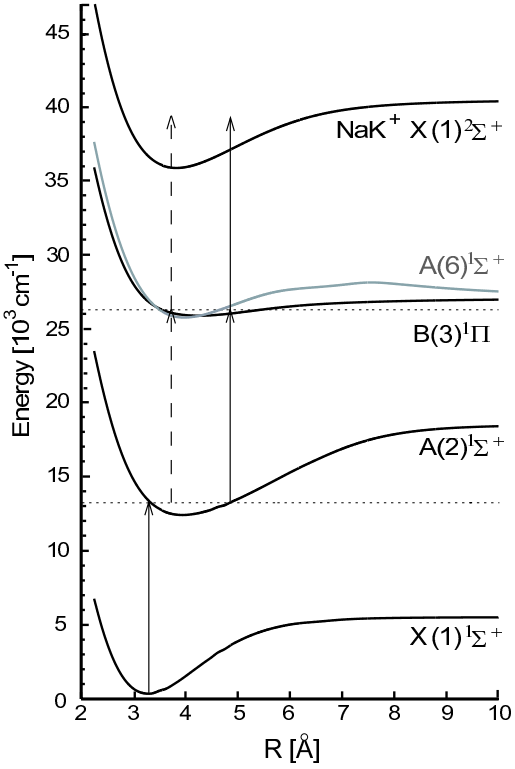

Figure 4.1: Potential energy surfaces of the NaK molecule (taken from [78]). The arrows symbolize favored nuclear distances for transitions, at the inner (dashed) and outer turning point.

Motivation for pulse cleaning. As Ref. [76] points out, for molecules where a positive correlation between the pulse peak intensity and total ion yield, such as NaK, exist an algorithm which maximizes the ionization efficiency senses no improvement in reducing certain amplitudes and makes no use of this particular control parameter [36]. This strongly constricts the amount of additional information which can be gathered from phase- and amplitude experiments compared to phase-only runs; they only converge slower due to the increased search space. Gaining no particular new information for the amplitude other than the profile of the input pulse, another method has to be thought of to unravel information about the importance of the employed, but "buried" vibronic transitions. Penalizing individuals for inherent amplitudes is a possibility, and in the following, the influence of the penalties on the ionization path will be studied.

4.1.2 Multi-objective approach(es)

Removing amplitudes from an already found solution does not deem the best answer because only the final niche will be subject to exploitation. Treating the experiment as an optimization of two separate goals (maximizing the ion yield while minimizing involved frequency components) has the advantage to regard the procedure as a multi-objective evolutionary algorithm (MOEA) [82] allowing to draw upon the knowledge and experience of this relatively new but rapidly expanding field of research and application[2].

The available multi-objective strategies divide into scalarization and Pareto methods (see Table 4.1.2). The main difference is *when* a decision about preference of

[2]a collection [83] holds 2667 bibliographic entries from the last few years

Scalarization Methods (a priori preference expression)	**Pareto methods** (a posteriori preference expression)
Compromise Programming	Exploration and Pareto Filtering
Weighted Sum Approach	*Weighted Sum Approach (Weight Scanning)*
Multiattribute Utility Analysis	Adaptive Weighted Sum method (AWS)
Physical Programming, Goal Programming	Normal Boundary Intersection (NBI)
Lexicographic Approaches	*Multiobj. Genetic Algorithms (MOGA)*
Acceptability Functions, Fuzzy Logic	Multiobj. Simulated Annealing (MOSA)

Table 4.1: Overview of multi-objective optimization strategies (taken from [84]), the methods written in italics are employed for this work.

goals is made, before or after the optimization. In femtochemistry, bond-selective optimizations involving product/branching ratios on CH_2BrCl [85], $CpFe(CO)_2Cl$ (where Cp means C_5H_5) [86], photofragmentation/ photoionization of $Fe(CO)_5$ [87], chemical conversion using actic acid ($CH_3CHOHCOOH$) [88], and isotope selective optimization[3] on K_2 [55, 89] can all be regarded as Weighted Sum Approaches.

For control pulse cleaning presented in this thesis, a Weighted Sum Approach with Weight Scanning, which counts as an *a posteriori*, Pareto method, is employed. To the author's knowledge, this concept has not been employed in the field of coherent control[4], so a brief introduction to the fundamentals will be given next.

4.1.3 Concept of Pareto-optimality

The idea of Pareto-optimality was brought up by the Italian sociologist, economist, and philosopher Vilfredo Pareto in the 19^{th} century, defining it as a macroeconomical state where no individual of a society can be better off, without impairing the welfare of another.

Fig. 4.2 illustrates this concept for a two-dimensional case, featuring the optimization goals f_1 and f_2, which both are to be minimized; for example cost and accident rate of a hypothetical car part. If to choose between the two manifestations A and B (of, say, a crankshaft) in the so-called "objective space"[5], no immediate advantage can be made out because one is better in f_1, but worse in f_2 and vice versa. To decide which part to choose, a meta-criterion would have to be employed for example safety regulations or ethical concerns. It is, on the other hand, easy to decide which of the two parts C and D to mount, because D is better than C in both objectives. Looking at the overview on the right, the three solutions A, B, and D can be said to constitute a provisional "Pareto-optimal front" (dashed line) - if no other solutions are known - they are also the "non-dominated" solutions[6].

[3] also described in Sec. 5.4.1

[4] earlier to [90], except for a recent theoretical investigation [91]

[5] contrary to the "decision space" $\vec{x}$

[6] non-domination will be discussed in Sec. 9.2

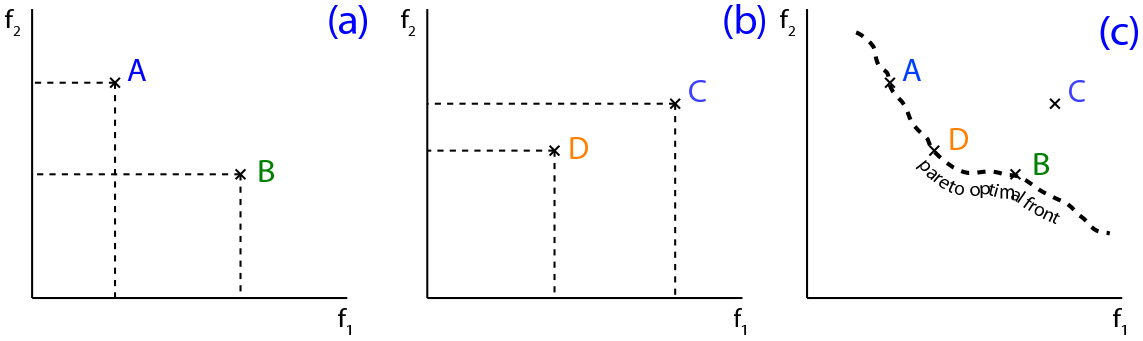

Figure 4.2: Compromise solutions in two dimensions, where both goals f_1 and f_2 are to be minimized. (a) shows two equivalent solutions, (b) a clear preference for D, and (c) a Pareto-optimal front consisting of three solutions that all outperform solution C.

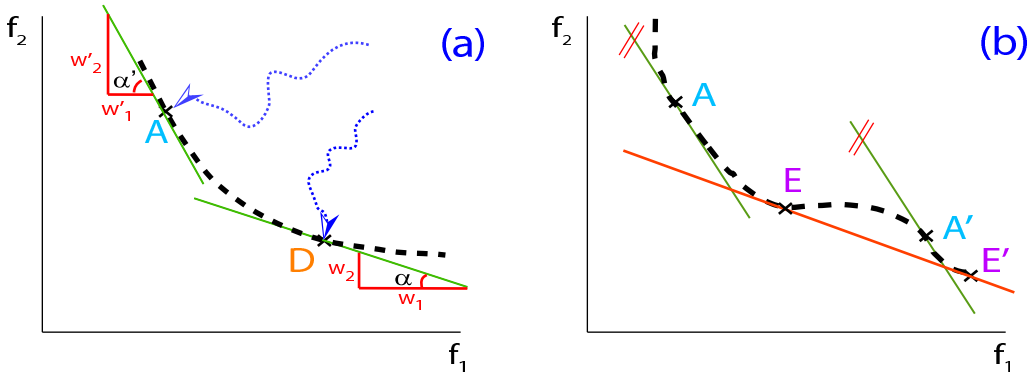

Figure 4.3: A Weighted Sum optimization with the weight vector (w_1, w_2) yields different solutions depending on the vector, and fails to provide unique solutions for non-convex Pareto-optimal fronts (b). The trails in (a) illustrate that the solutions are approached on different paths.

For a Weighted Sum approach with M goals, a general fitness function F consisting of a sum of partial fitnesses with weight w_j can be written as

$$F = \sum_{j=1}^{M} w_j \cdot f_j(\vec{x}). \tag{4.1}$$

whereby $f_j(\vec{x})$ are the functions of the individual objective variables $\vec{x}$.

The effect of the chosen cleaning strength vector w_j on the final optimal solution is outlined in Fig. 4.3. For the case (a), the final result of an algorithm run will be the unique solution D, as there the weighting will generate the lowest F. Choosing (w_1, w_2) differently would produce other solutions, such as A with (w_1', w_2'). Scanning the angle $\alpha = \arctan(w_2/w_1)$ will therefore yield the full Pareto-optimal front for repeated runs. Graph (b) depicts a non-convex front where such a weight scanning would fail to produce unique solutions (A and A', E and E').

4.2 Control Pulse Cleaning on NaK

For the experiment, the quadrupole mass spectrometer was set to the more abundant $^{23}Na^{39}K$ isotope, which was used thoughout this work if no isotope ratio experiment was conducted. The Spectra Physics Tsunami was used as laser source, having 120 fs to 180 fs pulse duration, a FWHM of 5 - 8 nm, a central wavelength of 770 nm, and pulse energies of about 10 nJ per pulse. The shaper employed was the SLM-256, used in phase- and amplitude modulation mode, and the time requirement for one generation was about 14 seconds. The NaK ion yield as first objective will be denoted as $f(T_i, \phi_i)$ or $f(\vec{x})$. To remove the unnecessary frequencies, the second objective is defined as "average transmission" like

$$T_a = \frac{1}{N} \sum_{i=1}^{N} T_i \tag{4.2}$$

where N denotes the number of pixels. A random initialization of the transmissions within an interval of [0,1] will have an expectation value of $\bar{T}_a$=0.5. It is the intention of control pulse cleaning to have a strong impact on the ionizations. There are power dependencies to the second or third order for two- or three photonic ionization, respectively, which requires choosing a cost function like

$$F(\vec{x}) = \frac{f(\vec{x})}{T_a^{\gamma}} \tag{4.3}$$

where γ is the cleaning exponent. This still can be considered a classical weighting approach as in Eq. 4.1 when calculating the logarithm

$$\log F = \underbrace{1}_{w_1} \cdot \underbrace{\log f(\vec{x})}_{f_1} + \underbrace{(-1) \cdot \gamma}_{w_2} \cdot \underbrace{\log T_a}_{f_2}. \tag{4.4}$$

As only the T_a^{γ} are weighted, w_1 is always 1, so for the further description w_2 can be referred just as $-\gamma$. Contrary to the above stated minimization example (the car part's cost and failure rate), for the following OCE, a maximization of the ion yield will be performed. In order to maximize both goals, the inverse average transmission $1/T_a^{\gamma}$ will be used in order to conform with the customary descriptions in the literature. For the experiments, the weight vector (w_1, w_2) was varied from (1,0) (no cleaning) to (1,-2) (strong cleaning) in steps of -0.5.

Fig. 4.4 shows the average transmission T_a versus tested individual (sorted by generation number), where a longer trail means a longer time of convergence. The curves all start at $\bar{T}_a$=0.5 and progress towards lower average transmissions, except for the $\gamma = 0.5$ case, which does not seem to be influencing the amplitudes much; and only a slight increase at the beginning and an otherwise gentle descent can be seen. There is a noticeable separation between all the cases. For $\gamma = 1.5$ a relatively strong decrease can be made out which is not too different than for $\gamma = 2$, they differ in their final convergence values, which is reached with much less amplitudes for the latter.

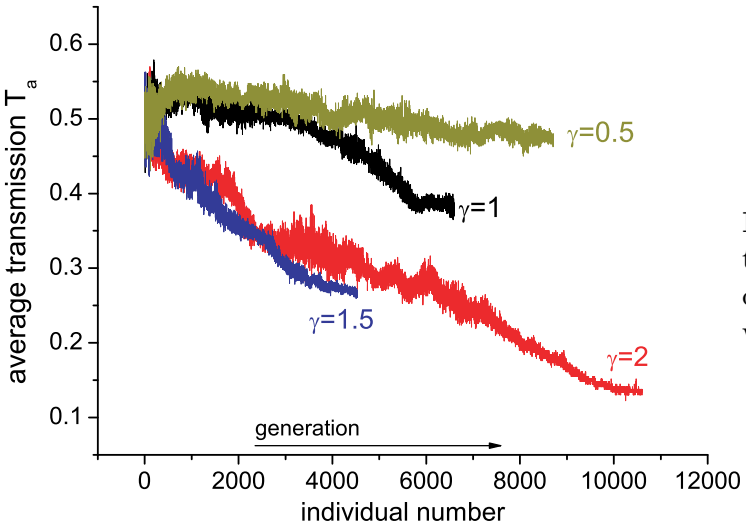

Figure 4.4: Development of the average transmission for different cleaning strengths γ, with increasing generation.

4.2.1 Frequency cleaning

An overview of the results in the time and frequency domain is provided by Fig. 4.5. The left column shows the effect of cleaning on the amplitudes for increasing cleaning strength (from top to bottom), similarly, the right column displays the resulting SFG-CCs.

The transmission values of the pixels are depicted as gray bars in the left column, they provide additional insight to the algorithm's inner working as they are directly encoded in the genotype[7]. From the patterns one can more clearly see the algorithm's "desire" to keep particular frequencies, even if there is not much intensity available from the Gaussian input beam[8]. An example of this behavior can be seen for the $\gamma = 1.5$ case, where the gray columns at 13041 and 13079 cm^{-1} do not have a high effect on the resulting spectral intensities, as similarly observed for the $\gamma = 2$ case at 13047 cm^{-1} (marked by arrows).

For the unconstrained optimization $\gamma = 0$, shown in the top row, almost all frequencies stay at high values, except for a "hole" around 13030 cm^{-1}. As progressing to higher cleaning strengths, the induced elimination of frequencies narrows the observed spectra and reveals distinct peaks, particularly for the $\gamma = 1.5$ case. The peaks can be assigned to transitions between vibrational levels of different electronic states of the $^{23}Na^{39}K$ isotope. Specifically, transitions between the $A(2)^1\Sigma^+ \leftarrow X(1)^1\Sigma^+$, $B(3)^1\Pi \leftarrow A(2)^1\Sigma^+$, and the $A(6)^1\Sigma^+ \leftarrow A(2)^1\Sigma^+$ states can be seen (marked on the left top of Fig. 4.5 and in Tab. 4.2).

An excitation process via the intermediate $B(3)^1\Pi$ state found by the cleaning experiment would agree with the results from Ref. [79] where, particularly for later sub pulses, wavepacket propagation seems to increase the total ion yield, also, indications of the $A(6)^1\Sigma^+$ state are present. In the temporal measurements and the cross-correlation traces, there is always one dominant structure for all cleaning strenghts, while the other features differ. This highlights the substantial influence of

[7]The spectral intensities can be considered as phenotype (as manifestation of the genetic makeup) because their shape is obtained by multiplying with input pulse's spectral distribution.

[8]The pattern extends further out, over 730 cm^{-1}, which is about three times the displayed range. The fitness functional was not adapted to the input pulse's spectrum in order to have a measure that represents the dimensioning of the shaper setup, not the (varying) laser bandwidth.

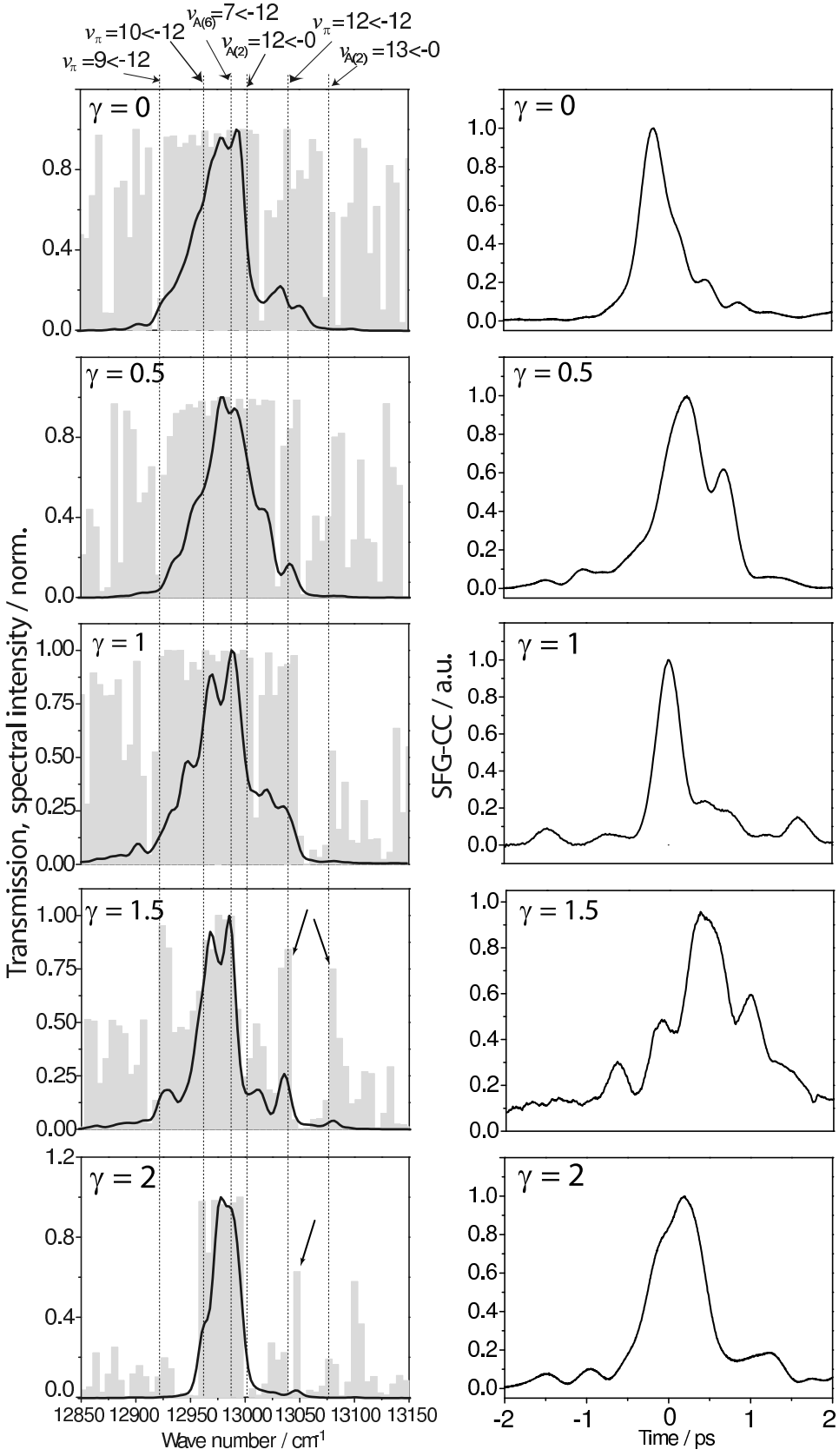

Figure 4.5: Pulse spectra (left column) and SFG-CCs (right column) when increasing the genetic pressure γ (top to bottom). The vertical lines indicate the assigned transitions between vibrational states of $A(2)^1\Sigma^+ \leftarrow X(1)^1\Sigma^+$, $B(3)^1\Pi \leftarrow A(2)^1\Sigma^+$, and $A(6)^1\Sigma^+ \leftarrow A(2)^1\Sigma^+$. The gray bars represent the transmissions of the respective pixels.

frequency / cm^{-1}	**transition**	**distinct peak visible for γ ?**
12922	v_π=9 ← 12	1.5, 2
12962	v_π=10 ← 12	1.5, 2
12988	$v_{A(6)}$=7 ← 12	1, 1.5, 2
13002	$v_{A(2)}$=12 ← 0	all, no distinct peak
13041	v_π=12 ← 12	all
13079	$v_{A(2)}$=13 ← 0	all, faint, from transmission patterns

Table 4.2: Identified vibronic transitions for NaK frequency cleaning.

the genetic pressure on the optimization path, and it is very well possible that the features that are revealed are brought about by the cleaning itself, and only come forward when the possibility to choose transitional states is strongly restricted. When surveying the temporal distances, a prominent pulse distance which amounts to 1.5 the oscillation period of the A(2)$^1\Sigma^+$ state is found, implying that the ionization occurs at the outer turning point of this potential[9]. For the $\gamma = 2$ case, where the spectra are most trimmed, a temporal broadening of the main sub pulse is prominent, which is an expected result when only a few pixels can contribute and little frequencies can interfere. From the pulse distances, a simple ionization scheme can be proposed where the population that is generated on the first excited A(2)$^1\Sigma^+$ state by either a pre-pulse or the main pulse, is ionized at the outer turning point after 660 fs by another pulse in a two-photonic process, whereby additional wave-packet dynamics on the B(3)$^1\Pi$ and A(6)$^1\Sigma^+$ might contribute, too. Still, a more detailed theoretical analysis such as [79] would be necessary at this point to grasp the temporal influence of the cleaning strength and the induced dynamics.

4.2.2 Cleaning strength dependent fitness

The influence of the cost function on the resulting optimization factors is shown in Fig. 4.6. The error of the optimization factors is determined to be about 10%. For (a), the final values are normalized to the optimization factor when no cleaning is applied (relative to an unshaped pulse) which was f_0=1.4 for the relatively narrow bandwidth of the Tsunami. For lower cleaning strengths, the final results do not differ much from the original factor. At γ=1.5, already a significant impact and a much lower factor of f/f_0 =0.3 is observed, and even less for $\gamma = 2$.

Another question is how the optimized results would perform if they competed with an unshaped pulse on the same power level, as all optimized pulse shapes are reduced in power due to the elimination of amplitudes. For this comparison, the unshaped reference pulse was reduced in power using a flat transmission function. As depicted in Fig. 4.6 (b), interestingly, the pulses originating from a higher cleaning strength perform better as their power-reduced, unshaped counterparts, highlighting the importance of the induced (or unravelled) wave packed dynamics,

[9]Distances of 0.5 T$_{osc}$ would be difficult to resolve with the employed pulse length, but could be embedded within the more elongated main pulses.

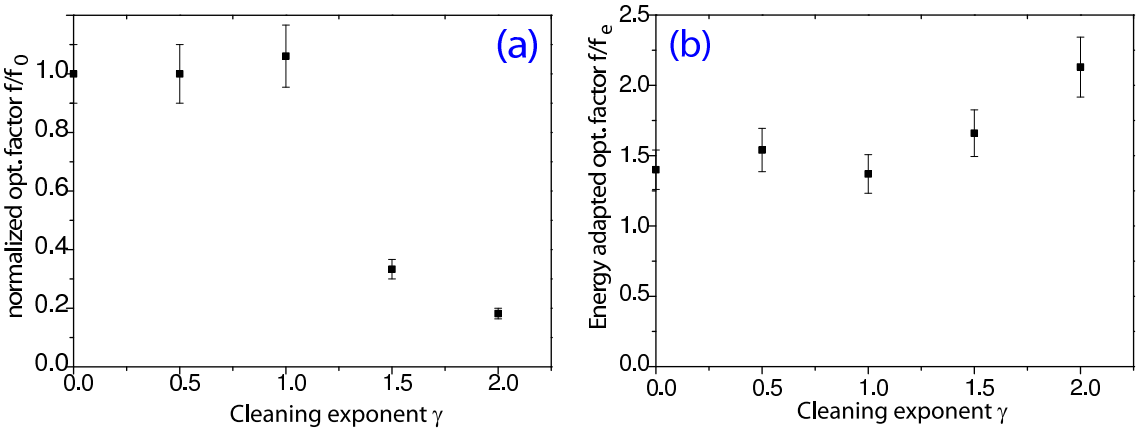

Figure 4.6: Optimization factors for different cleaning strengths. (a) Optimization factor f/f_0 relative to the factor of an unrestrained run; (b) Optimization factors f/f_e compared to an unshaped pulse at the same power level.

up to a factor of $f/f_e = 2.13$ for γ=2. This means that cleaning goes along with an increased efficiency; apparently due to the allocation of the available energy to the most relevant states, emphasizing the usefulness of this method.

4.2.3 Pareto-optimal front for NaK cleaning

Using the translation f/f_0 as f_1, and $1/T_a$ as f_2, the solutions can be embedded in objective space in the fashion of Figs. 4.2 and 4.3, whereby here, both objectives are to be maximized. To observe the progress, the two fitness values were stored for every tested individual during the experimental runs.

Fig. 4.7 overlays two runs in objective space (gray dots represent individual solutions from γ=0.5, and black dots from $\gamma = 1.5$) together with the Pareto-optimal solutions (black rectangles with error bars) for all performed cleaning strengths. The fact that the Pareto optimal solutions recorded from the last generation do not lie on the upper slope must be attributed to the experimental noise. The objective space plot shows which combinations of fitnesses are possible, and therefore provides a correlation between the conflicting objectives: ion yield and power. The trade-off between ionization efficiency and the effort to do it with as little amplitudes as possible can be seen in the location of the solutions in objective space: for $\gamma = 0.5$, a high ion yield was achieved, but with effectively no reduction of frequencies, for $\gamma = 1.5$, less frequencies are involved ($1/T_a$=3.69) at a reduced ionization yield.

During the experiment, the solutions develop differently, which is visualized in Fig. 4.8 by calculating the average coordinate (like the center of mass) of one generation $(\bar{f}_1, \bar{f}_2)$. For $\gamma = 0.5$, a trend strictly upwards is observed, without paying much attention to pulse cleaning. For $\gamma = 1.5$, the curve "bends" at generation 18, where the highest ion yield for this particular cleaning strength is achieved. Such a bend is a very good sign of a balanced choice of cleaning strength, because if one objective is dominant, a much straighter approach to the Pareto-optimal solution is the case, as observed for $\gamma = 0.5$.

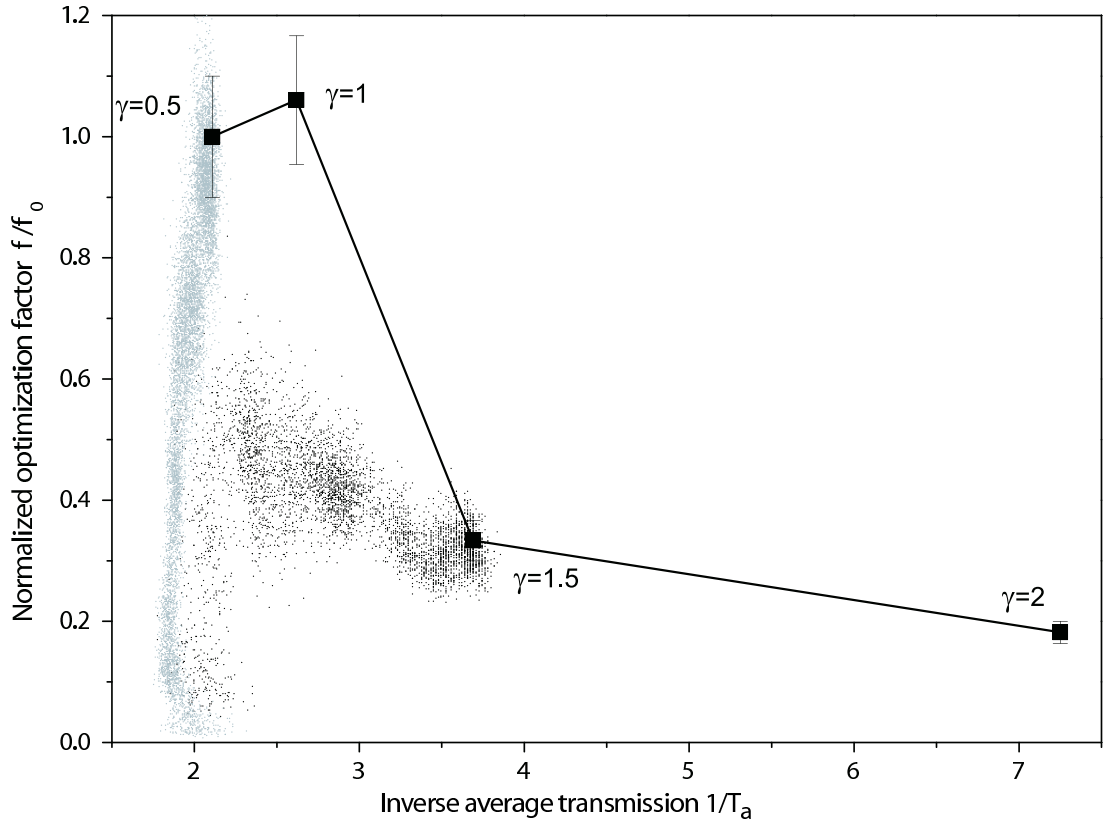

Figure 4.7: Pareto-optimal front drawn from the solutions of four γ's and two full featured courses. The gray dots represent γ=0.5, and the black γ=1.5. The x-coordinate is the inverse of the average transmission $1/\mathrm{T}_a$, and the y-coordinate is the pulse shape dependent ion yield $f(T_i, \phi_i)$.

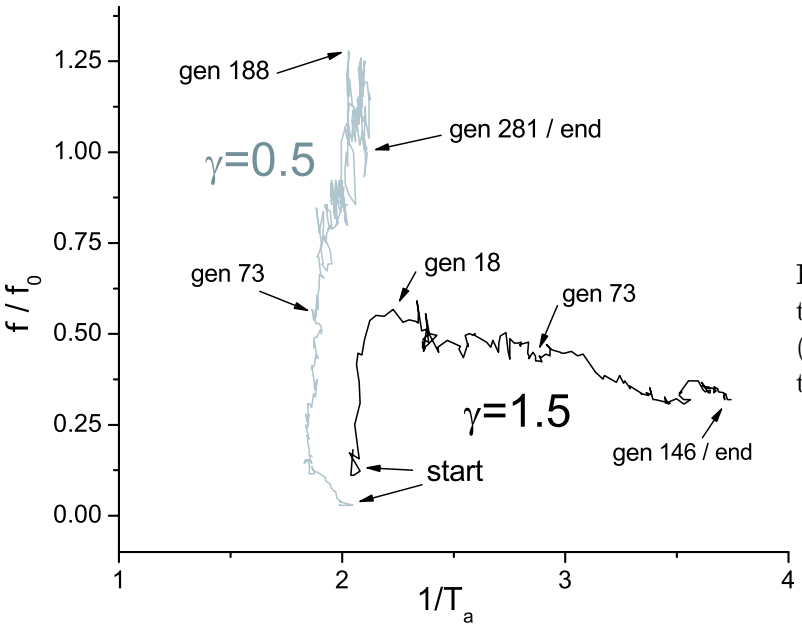

Figure 4.8: Courses of the center of fitness $(\bar{f}_1, \bar{f}_2)$ (averaged over one generation), for γ=0.5 and γ=1.5.

4.3 Summary and Outlook

In this chapter a new method of revealing transition frequencies for coherent control experiments was described. By influencing the selection process, customized objectives can be incorporated as cost functions. An experiment, reducing less important transition frequency components of a NaK ionization optimization was incorporated into the framework of multi-objective evolutionary algorithms (MOEA) as a Scanning Weighted Sum Approach which allowed to display the results from the experiments in objective space and construct a Pareto-optimal front.

The spectra of the Pareto-optimal solutions revealed transitions between different electronical states, which are usually hidden in ordinary optimizations. This demonstrates that the method is feasible for extracting new information from quantum control experiments, provided that one keeps in mind that genetic pressure might lead to strong changes to the ionization path. Quantitatively, it was found that the best cleaning factor for the employed three-step photoionization of NaK lies around 1 and 1.5, this may of course change with the examined molecular system and with different, employed non-linearities.

Cost functionals are not restricted to particular deliberations, weight factors can be chosen with a vast variety of ulterior motives, recently demonstrated by "cleaning" the signal-to-noise level [92].

Other goals, for example, short term noise versus long term stability could be improved, or the reproducibility of a solution versus complexity. A local search in objective space could also be an interesting approach, when a particular area is selected as a target.

A very promising feature would be the implementation of a modern multi-objective algorithm. They are able, by design, to retrieve the Pareto-optimal front within a single run, without the need to specify weightings. The implementation of such an algorithm for retrieving polarization pulse shapes will be described in Chapter 9.